

Formation of Ideal Rashba States on Layered Semiconductor Surfaces Steered by Strain Engineering

Wenmei Ming,^{†,‡} Z. F. Wang,^{†,§} Miao Zhou,^{†,||} Mina Yoon,^{*,‡} and Feng Liu^{*,†,‡}

[†]Department of Materials Science and Engineering, University of Utah, Salt Lake City, Utah 84112, United States

[‡]Center for Nanophase Materials Sciences, Oak Ridge National Laboratory, Oak Ridge, Tennessee 37831, United States

[§]Hefei National Laboratory for Physical Sciences at the Microscale, University of Science and Technology of China, Anhui 230026, China

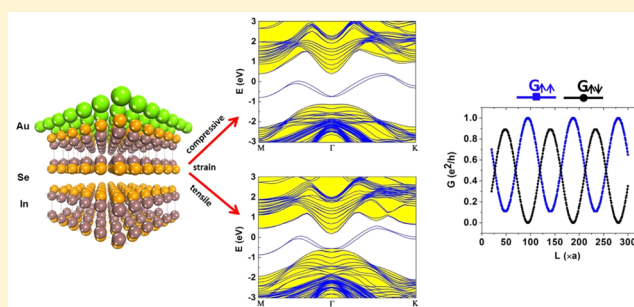
^{||}Key Laboratory of Optoelectronic Technology and Systems of the Education Ministry of China, College of Optoelectronic Engineering, Chongqing University, Chongqing 400044, China

[±]Collaborative Innovation Center of Quantum Matter, Beijing 100084, China

Supporting Information

ABSTRACT: Spin splitting of Rashba states in two-dimensional electron system provides a promising mechanism of spin manipulation for spintronics applications. However, Rashba states realized experimentally to date are often outnumbered by spin-degenerated substrate states at the same energy range, hindering their practical applications. Here, by density functional theory calculation, we show that Au one monolayer film deposition on a layered semiconductor surface β -InSe(0001) can possess “ideal” Rashba states with large spin splitting, which are completely situated inside the large band gap of the substrate. The position of the Rashba bands can be tuned over a wide range with respect to the substrate band edges by experimentally accessible strain. Furthermore, our nonequilibrium Green’s function transport calculation shows that this system may give rise to the long-sought strong current modulation when made into a device of Datta-Das transistor. Similar systems may be identified with other metal ultrathin films and layered semiconductor substrates to realize ideal Rashba states.

KEYWORDS: Ideal Rashba splitting, layered semiconductor substrate, heavy metal overlayer, strain, spin field transistor



Rashba states refer^{1,2} to spin splitting of two-dimensional (2D) electronic states as a result of perpendicular potential asymmetry in the presence of spin–orbit coupling (SOC). Much recent effort has been made in searching for this type of electronic states in solid state systems for potential spintronics applications, such as spin field transistor³ and intrinsic spin Hall effect.⁴ The degree of spin splitting, quantified by the Rashba parameter α , scales with the gradient of perpendicular potential asymmetry and strength of SOC. The earliest realization of the Rashba states was made in the asymmetric quantum well formed in InGaAs/InAlAs heterostructure⁵ with small spin splitting. Noble metal (e.g., Au,⁶ Ag,⁷ and Ir⁸) and *sp*-orbit heavy-metal surfaces (e.g., Bi,⁹ Sb,¹⁰ and Pb¹¹) were shown to have large spin splitting. Heavy metal adatoms alloying with metal (e.g., Bi/Ag(111)¹²) and/or semiconductor surfaces (e.g., Bi/Si(111)¹³) were found to possess giant spin splitting. Most recently, new surface systems with Rashba states have been reported in graphene/Ni(111)¹⁴ and molecule-adsorbed topological insulators.^{15–17} However, because the substrates previously adopted are either metal or semiconductor with substantial surface states, typically Rashba states are overwhelmed by the large number of spin-degenerated substrate states at the same energy window, so

that the desired transport of Rashba-state carriers cannot be isolated from the substrate carrier contribution, hindering their practical applications.

The effort of overcoming this limitation therefore needs to be directed to tuning the relative energy positioning between the Rashba bands and the substrate bands, in such a way that Rashba bands have significant spin splitting from the strong interaction with the substrate, while they stay separated from the substrate bands in energy. The ideal case is that the Rashba bands are completely situated inside the band gap of the substrate, so that the pure transport contributed by only Rashba states can be obtained. To the best of our knowledge, such ideal Rashba states were only realized on Te-terminated surface of BiTeX (X = I, Br, and Cl).^{18,19} In this Letter, using density functional theory (DFT) calculations, we demonstrate a new approach to realize ideal Rashba states in a hybrid system [Au/InSe(0001)] of Au one monolayer film deposition on a completely different type of substrate, that is, layered large band gap semiconductor β -

Received: October 1, 2015

Revised: December 1, 2015

Published: December 10, 2015

InSe(0001), which is a naturally saturated surface without any dangling bonds as encountered in conventional semiconductor surfaces. We show that the separation between Rashba bands and substrate bands can be further tuned via strain exerted on the substrate. We show potential application of our system for spin-field transistor by quantum transport calculation.

Our DFT calculations are carried out with projector augmented wave pseudopotential²⁰ in the VASP package.²¹ Perdew–Burke–Ernzerhof (PBE)²² exchange–correlation functional and DFT-D2²³ correction of van der Waals (vdW) interaction are used for obtaining accurate geometry of layered InSe(0001). A 450 eV kinetic energy cutoff and $11 \times 11 \times 1 \Gamma$ centered k-mesh sampling are adopted for total energy convergence. The substrate is simulated by seven layers slab of (1×1) -InSe(0001) with an experimental in-plane lattice constant a of 4.05 Å and an vacuum layer of more than 20 Å. All the atoms are relaxed until the forces are smaller than 0.01 eV/Å. The screened HSE (Heyd, Scuseria, and Ernzerhof)²⁴ hybrid functional is subsequently adopted for reliable substrate band gap and positioning of Rashba bands with SOC.

Bulk β -InSe has a hexagonal layered crystal structure with each layer consisting of Se–In–In–Se atomic planes and stacking along the z -direction. Within each layer, In and Se are bonded covalently; between layers, they are bonded with vdW interaction. Our HSE calculation shows that InSe(0001) has a large band gap of 1.28 eV (see Figure S1 in Supporting Information), which is very close to the bulk experimental value of 1.35 eV.²⁵ The apparent absence of surface bands in the band gap due to the saturated layered structure of InSe(0001) is also verified from the calculated band structure. Besides, we note that Au ultrathin films^{26–28} including one monolayer thickness on InSe(0001) were successfully grown in experiment and intensively studied in photovoltaics due to the formation of abrupt Schottky interface between Au overlayer and InSe(0001), which makes our study of Au/InSe(0001) in the context of Rashba states even more relevant to experimental feasibility.

The atomic structure of Au/InSe(0001) is shown in Figure 1a,b for side and top views, respectively, that consists of one

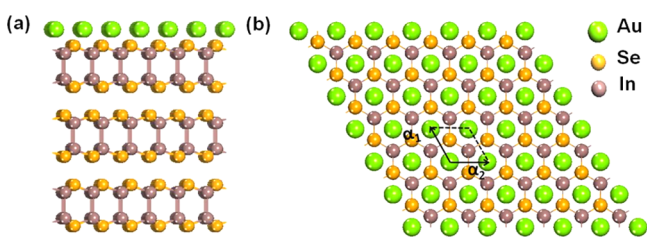


Figure 1. (a) Side view of the structure of Au monolayer film deposition on β -InSe(0001) substrate, which is shown with only the top three layers for clarity. (b) Top view of the structure; α_1 and α_2 represent the surface unit cell vectors.

monolayer Au thin film on InSe(0001). The site directly above the hollow position of both the topmost Se and In atomic planes is energetically favorable for Au adsorption. The interlayer binding energy between Au and InSe(0001) is 0.58 eV/surface-unit-cell. It indicates that the surface interaction is in an “intermediate” range,²⁹ slightly stronger than vdW bond but significantly weaker than typical chemical bond. Figure 2a shows the corresponding band structures of Au/InSe(0001) along M– Γ –K directions. Bands located in the shaded areas represent the ones from substrate states, while the ones located in the gap between them are characterized as the ones from surface states.

The characterization of those bands will be further discussed later. The two surface bands show a large Rashba spin splitting at the k -points from midpoint of M– Γ to midpoint of Γ –K and are completely inside the substrate band gap. Therefore, this system has the ideal Rashba states immune to the substrate states.

Meanwhile, in the vicinity of Γ the Rashba surface bands are only ~ 0.25 eV above the valence band maximum (VBM) of the substrate. Next, we apply both compressive and tensile biaxial strains to the substrate in order to tune the relative position of the surface bands and the substrate bands through the difference in their deformation potential.⁴⁴ Compressive biaxial strain is found to separate even further the surface and substrate bands, and the surface bands becomes ~ 0.40 eV above the VBM under a compressive strain of -1.2% , as shown in Figure 2b. At -2.4% compressive strain, the surface bands becomes ~ 0.5 eV (see Supporting Information Figure S2) above VBM. It can be attributed to the substrate band gap enlargement and the down-shifting and up-shifting of VBM and conduction band maximum (CBM), respectively, relative to the surface bands (see Supporting Information Figure S2). In contrast, tensile strain exerts an opposite effect that the surface and substrate bands become increasingly closer and then overlapped, as seen under a tensile strain of $+2.4\%$ in Figure 2c, because the band gap shrinks and the VBM up shifts and CBM down shifts.

Previous DFT and tight-binding calculations^{25,31} reported that the VBM of InSe is composed of the bonding state by p_z orbitals of Se and In, and the CBM is composed of antibonding state by s and p_z orbital of Se and s orbital of In. Moreover, with increasing compressive strain the energy levels of the VBM bonding state and CBM antibonding state will become lower and higher, respectively, due to decreased In–Se distance and thereby increased overlap integral between these orbitals compared with the strain-free case. This trend will be reversed under increasing tensile strain, which causes increased In–Se distance and thereby decreased overlap integral. Therefore, it is observed from our band structure results that InSe(0001) band gap increases under compressive strain and decreases under tensile strain. Besides, the interlayer Au–Se distance keeps increasing under compressive strain and decreasing under tensile strain (Supporting Information Figure S3), Au onsite energy hence should be raised and lowered under compressive and tensile strains, respectively. Consequently, the Rashba bands are lifted higher under compressive strain and lower under tensile strain. Combining the three trends for VBM, CBM, and Rashba bands together, it becomes clear that we can further isolate the Rashba bands from InSe(0001) with compressive strain but the opposite with tensile strain.

Because of the larger separation of the Rashba bands from VBM on -1.2% strained substrate than on strain-free case, we choose the -1.2% strained substrate with lattice constant a of 4.00 Å in all the following results. We have identified the asymmetric potential responsible for the Rashba spin splitting and the nonzero Rashba parameter $\alpha \propto \int \partial V(z)/\partial z dz$.³² The in-plane averaged potential along the stacking direction z , $V(z) = (1/A) \int V(x, y, z) dx dy$, where A is the surface area, is shown in Figure 3a. The red dashed box highlights the region of Au and the first layer of the substrate, where electrons experience an asymmetric potential. In the remaining region, however, the potential is symmetric and almost identical at each layer. This implies that the local asymmetric potential induces localized Rashba states only in the top Au + InSe layer. To confirm this, in Figure 3b–e we show the local charge distribution for the Rashba states 1–4 as labeled in Figure 2b, at each atomic plane from the

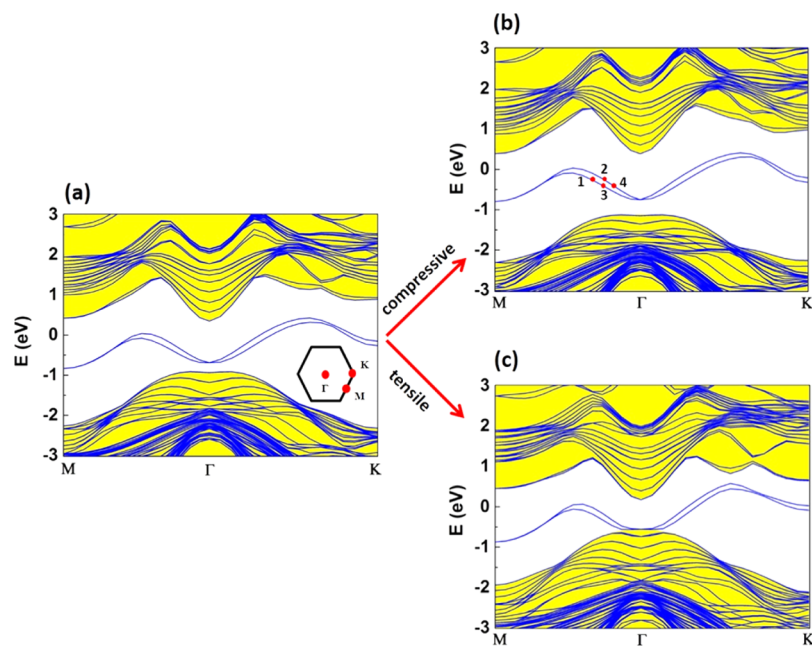


Figure 2. Band structures of Au/InSe(0001) under different substrate strains. (a) Strain-free lattice constant $a = 4.05$ Å. The inset is the schematic of the 2D hexagonal Brillouin Zone for Au/InSe(0001). (b) Compressive strain = -1.2% at $a = 4.00$ Å. (c) Tensile strain = $+2.4\%$ at $a = 4.15$ Å. In (b), labels 1 and 2 are two representative Rashba states with energy $E = -0.28$ eV and labels 3 and 4 with $E = -0.40$ eV.

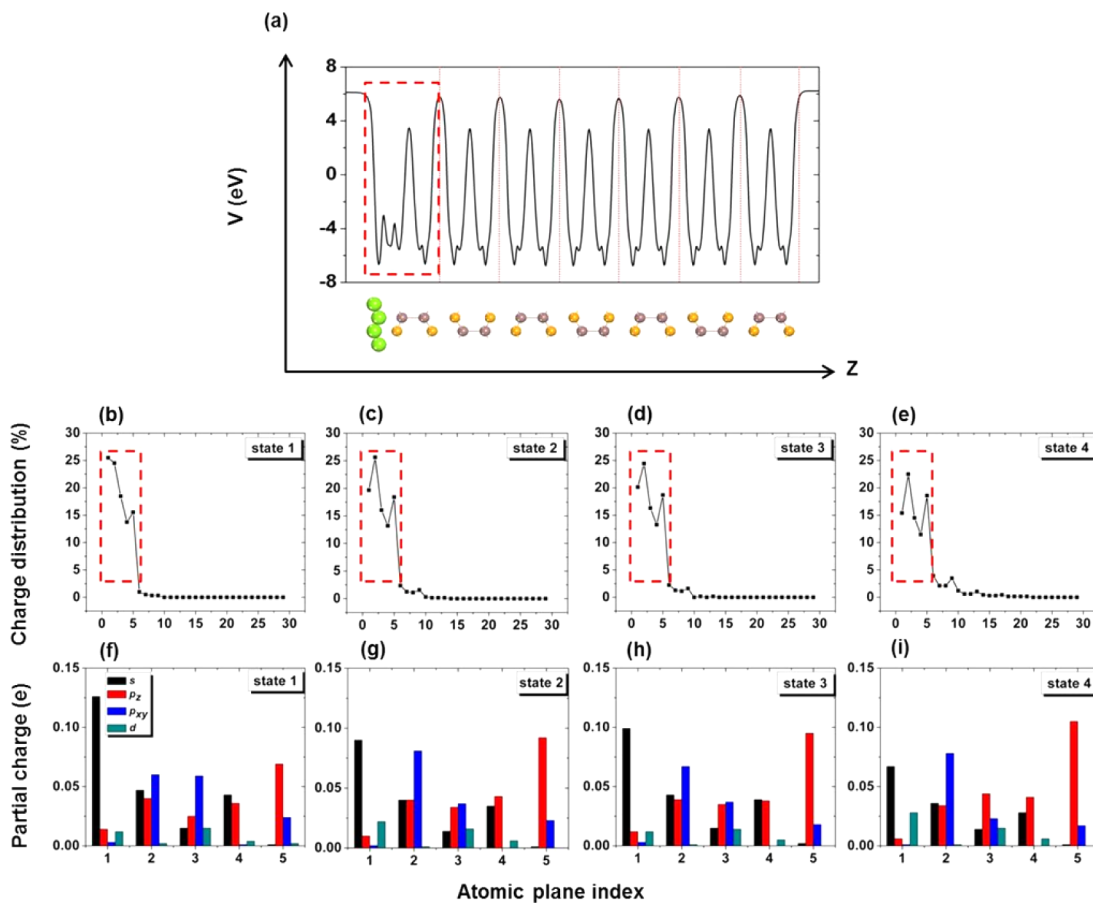


Figure 3. (a) Plane-averaged potential V along z -axis. (b–e) Charge distribution of the Rashba states 1–4, as labeled in Figure 2b as a function of atomic plane. (f–i) Orbital compositions in the first five atomic planes for the Rashba states 1–4. The red-dashed boxes highlight V only at the first five atomic planes. The red dotted lines in (a) represent the vdW spacing positions between InSe(0001) layers.

topmost Au to the bottommost Se plane. The red dashed boxes show that the charge of each state is mostly distributed in the top five atomic planes, beyond which it is negligibly small.

Microscopically, tight-binding Hamiltonian was adopted to understand Rashba spin splitting in simple systems such as graphene^{33,34} and Au(111),^{35,36} where the effect of asymmetric potential is included by adding nonzero intersite and intrasite hopping matrix elements between orbitals, which otherwise have zero hopping matrix elements. In order to have nonzero intrasite hopping matrix elements under asymmetric potential along the z -direction, the Rashba wave function must contain orbitals with opposite parities such as s/p_z and p_z/d_{z^2} at heavy atoms (see Supporting Information Figure S5 and Table S1 for the analysis of intrasite s/p_z hybridization leading to Rashba splitting). This is confirmed in Figure 3f–i by plotting orbital compositions of the Rashba states 1–4 at Au site, which all contain a large amount of s , and a small amount of p_x, p_y and d_{z^2} components at Au atomic plane. While it is difficult to have a simple picture for Au/InSe(0001) on the induced intersite hopping, which in graphene and Au(111) is from nearest-neighbor σ – π hybridization between $p_{x,y}$ and p_z orbitals under asymmetric potential, the existence of $p_{x,y}$ and p_z orbitals at each atomic plane particularly at Se plane may still indicate the contribution from intersite hopping to the Rashba spin splitting observed in Au/InSe(0001).

Furthermore, we show the spin polarization texture of the Rashba states in Figure 4. The spin polarization is defined as $\vec{p}(\vec{k})$

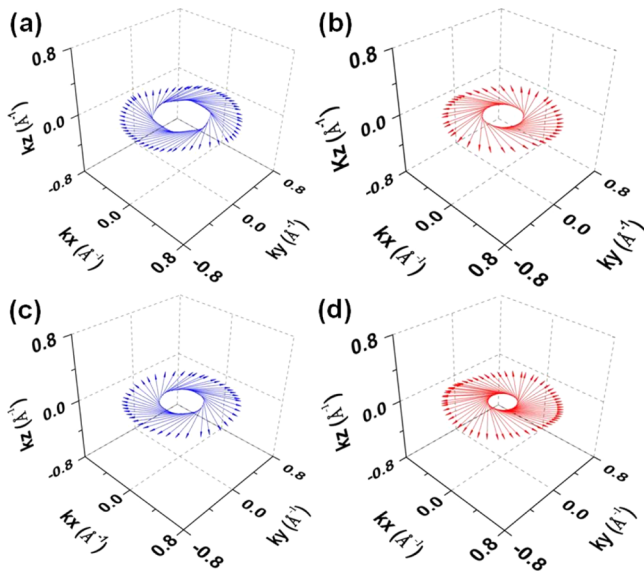


Figure 4. Spin polarization textures of the Rashba bands at 2D iso-energy arcs with $E = -0.28$ eV (a,b) and $E = -0.40$ eV (c,d), respectively. (a,c) The outer circle of corresponding iso-energy arc and (b,d) are from the inner circle of corresponding iso-energy arc.

$= [\langle S_x(\vec{k}) \rangle, \langle S_y(\vec{k}) \rangle, \langle S_z(\vec{k}) \rangle]$, where $\langle S_\alpha(\vec{k}) \rangle = \langle \varphi(\vec{k}) | \sigma_\alpha | \varphi(\vec{k}) \rangle$, ($\alpha = x, y, z$). It is plotted at two iso-energy (E) arcs of $E = -0.28$ eV and -0.40 eV. Blue and red colors represent outer and inner branches of the Rashba bands, respectively. Overall, the iso-arc is isotropic for the inner circle with smaller k -vector but gains some anisotropy of hexagonal shape for the outer circle with larger k -vector. The z -component of the spin polarization is about ten times smaller than the x - and y -components, and the xy -plane spin polarization is nearly perpendicular to the k -vector. This spin polarization texture is very similar to that in 2D Rashba SOC free-electron gas, which has only in-plane spin components.³⁷

Because the spin polarization texture represents the effective distribution of k -dependent magnetic field generated by SOC³⁸ under perfect 2D Rashba SOC as in 2D Rashba SOC free-electron gas, the spin of an initially spin-up polarized electron shows sinusoidal oscillation over its travel length.³⁹ We thus expect that Au/InSe(0001) should possess similar spin oscillation effect. We fit our Rashba bands around Γ point to the free-electron Rashba band dispersion. The fitted Rashba parameter α is 0.45 eV Å. It corresponds to a characteristic spin precession length⁴⁰ $L_{so} = (\pi\hbar^2/2m\alpha)$ of 50 Å, over which electron up-spin is rotated to down-spin, where m is the electron effective mass. The periodicity of the sinusoidal oscillation then is $2L_{so} = 100$ Å.

Next, we proceed to show the electron spin oscillation effect in Au/InSe(0001) by calculating its spin-dependent electron conductance. Because the Rashba bands are isolated far away from the substrate band edges, we can write an effective tight-binding Hamiltonian for only the two Rashba bands, neglecting the other bands. The effective tight-binding Hamiltonian is obtained by using the two maximally localized Wannier functions as the basis set constructed with the Wannier90 package.⁴¹ A two-terminal nanoribbon Datta-Das transistor with the width of $4a$ is shown in Figure 5a. The left lead is spin-up ferromagnetic and the right lead is aligned with the left lead in either parallel or antiparallel configuration.⁴² We assume no SOC in the lead regions by artificially setting the spin-flip elements in the Hamiltonian matrix to zero, and the channel region has the SOC as described by the full effective Hamiltonian. Figure 5b shows the band structure of the nanoribbon representing the channel region.

The spin-dependent electron ballistic conductance $G(E_F)$ of the device is calculated with nonequilibrium Green's function (NEGF) method in Landauer-Büttiker formalism⁴²

$$G_{pq}(E_F) = \frac{e^2}{h} \text{Tr}(\Gamma_p^R G^R \Gamma_r^L G^A) \quad (1)$$

where Γ is the interface coupling matrix between the lead and the channel and is related to the channel self-energy (Σ^R) by $\Gamma = i(\Sigma^R - \Sigma^A)$, $G^R = G^{A\dagger}$ is retarded Green function of the channel, p, q are spin indexes and l, r denote the left and right leads, respectively. Because in this work we focus on the intrinsic modulation of the spin-polarized current by the Rashba SOC, we do not include the interfacial effects between lead and channel, disorder and/or impurities. We purposely choose the Fermi energy (E_F) to be at either of the two red dashed lines in Figure 5b, crossing only the two Rashba bands (R_1) when $E_F = E_1$ or two sets of Rashba bands ($R1, R2$) plus the spin almost degenerated bands when $E_F = E_2$.

In Figure 5c, $G_{\uparrow\uparrow}(E_F = E_1)$ and $G_{\uparrow\downarrow}(E_F = E_1)$ are plotted for the spin-up and spin-down conductances at the right lead, respectively, as a function of channel length (L). They both exhibit nearly perfect sinusoidal oscillation with periodicity of $\sim 90a$ (~ 360 Å). This oscillation periodicity from the nanoribbon configuration was ~ 3.6 times as large as that estimated from the 2D configuration. We confirmed this increased oscillation periodicity by again fitting the nanoribbon band structure around Γ to the free-electron Rashba band dispersion. We found that the Rashba parameter α is reduced to 0.25 eVÅ and the effective mass m is reduced to be about half of that for 2D configuration. Therefore, the oscillation periodicity $2L_{so}$ was increased by 3.6 times, which is consistent with the increase from the conductance calculation. We noticed that previously when estimating the Rashba parameter α in 2D structure we only

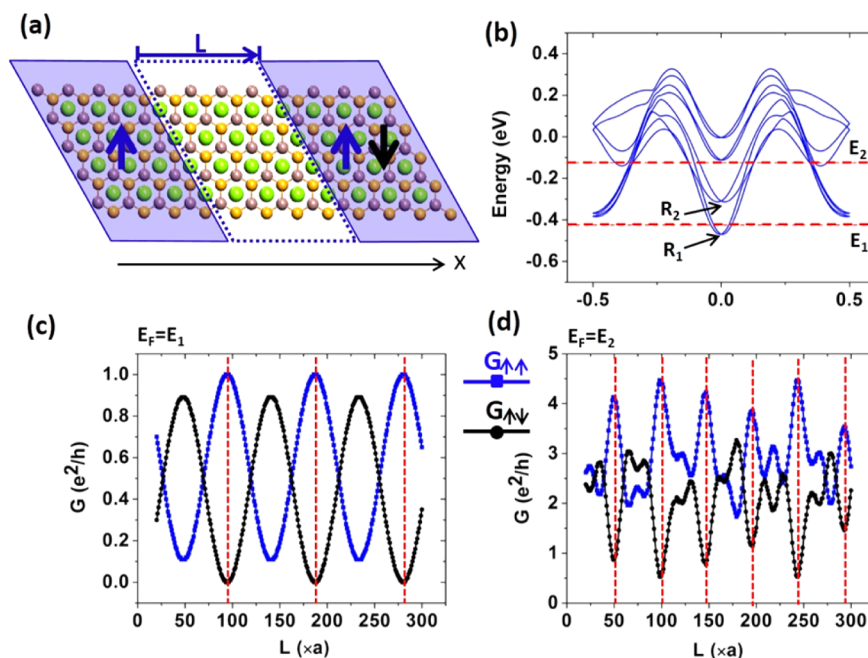


Figure 5. (a) Datta-Das transistor: the left and right boxes represent the source and drain leads without SOC, respectively. Both leads are ferromagnetic with their spins (shown as arrows) aligned either parallel or antiparallel. The middle box represents the conducting channel with SOC. (b) Band structure of the nanoribbon channel. (c,d) The spin-up $G_{\uparrow}(E_F)$ and spin-down $G_{\downarrow}(E_F)$ as a function of channel length (L) in units of lattice constant a . The vertical dashed lines label the conductance peak positions.

included the Rashba split bands around Γ but neglected the almost spin degenerated bands at the same energy range around M . However, when in 1D nanoribbon structure, the bands around M in 2D structure could be folded to around Γ and hence result in the modified Rashba band dispersion and the decrease of α and m . In addition, we purposely shifted E_F to E_2 and show $G_{\uparrow}(E_F = E_2)$ and $G_{\downarrow}(E_F = E_2)$ in Figure 5d. They exhibited strong oscillation but with smaller periodicity of $\sim 50a$ ($\sim 200 \text{ \AA}$) compared to that when $E_F = E_1$. It is different that the oscillation does not follow well a sinusoidal curve. Noticing that Rashba bands R_2 have a larger Rashba parameter α of 0.45 eV \AA than R_1 , and the interband interference between R_1 and R_2 should also appear when E_F crosses both of them, the overall oscillation therefore becomes less regular and has smaller periodicity.

Lastly, we point out that the compressive strain on the substrate, which is critical for improving the ideality of the Rashba bands in Au/InSe(0001), can be achieved by epitaxially growing InSe(0001) film on an additional semiconductor substrate with smaller lattice constant. Several substrates such as GaAs(111), AlAs(111), ZnSe(111), and Ge(111) all have the surface lattice constant of $\sim 4.00 \text{ \AA}$ and hence impose desirable amount of compressive strain of -1.2% on InSe(0001). On the other hand, InSe(0001) can be replaced by other layered semiconductor substrates such as those from metal chalcogenides family⁴³ (e.g., γ -InSe, α -In₂Se₃, β -In₂Se₃, 2H-MoS₂), and they may also exhibit ideal Rashba states upon heavy metal deposition such as Bi, Pb, Tl, Sb, and Au as the overlayers.

In conclusion, using DFT electronic structure calculations, we have demonstrated the formation of the long-sought ideal Rashba states in Au monolayer film deposition on a new type of substrate, that is, layered semiconductor surface β -InSe(0001). They are situated completely inside the substrate band gap, in the same fashion as the recently studied surface topological states,^{44,45} and possess large spin splitting. The ideality of the Rashba bands can be tuned over a wide range with respect to the

substrate band edges with experimentally accessible strain. Furthermore, the desired property of strong modulation of spin-polarized current in Datta-Das transistor setup is confirmed by NEGF transport calculations.

■ ASSOCIATED CONTENT

Supporting Information

The Supporting Information is available free of charge on the ACS Publications website at DOI: 10.1021/acs.nanolett.5b04005.

Substrate band gap, energy separation between Rashba surface bands and substrate band edges, distance between Au and InSe(0001), Rashba parameter α , band widths, and Wannier fitting. (PDF)

■ AUTHOR INFORMATION

Corresponding Authors

*E-mail: myoon@ornl.gov (M.Y.).

*E-mail: fliu@eng.utah.edu (F.L.).

Notes

The authors declare no competing financial interest.

■ ACKNOWLEDGMENTS

The work at Utah was supported by NSF MRSEC (Grant DMR-1121252) (W.M., Z.F.) and DOE-BES (Grant DE-FG02-04ER46148) (M.Z. F.L.); the work at Oak Ridge National Laboratory was supported by the Laboratory Directed Research and Development Program (W.M.) and by the Center for Nanophase Materials Sciences (M.Y.) of the Scientific User Facilities Division, Office of Basic Energy Sciences, U.S. Department of Energy. We thank the CHPC at the University of Utah for providing the computing resources. This research used resources of the National Energy Research Scientific Computing Center, supported by the Office of Science of the

U.S. Department of Energy under Contract No. DE-AC02-05CH11231.

REFERENCES

- (1) Rashba, E. I. *Sov. Phys. Solid State* **1960**, *2*, 1109.
- (2) Bychkov, Y. A.; Rashba, E. I. *JETP Lett.* **1984**, *39*, 78.
- (3) Datta, S.; Das, B. *Appl. Phys. Lett.* **1990**, *56*, 665.
- (4) Sinova, J.; Culcer, D.; Niu, Q.; Sinitsyn, N. A.; Jungwirth, T.; MacDonald, A. H. *Phys. Rev. Lett.* **2004**, *92*, 126603.
- (5) Nitta, J.; Akazaki, T.; Takayanagi, H. *Phys. Rev. Lett.* **1997**, *78*, 1335.
- (6) LaShell, S.; McDougall, B. A.; Jensen, E. *Phys. Rev. Lett.* **1996**, *77*, 3419.
- (7) Popovic, D.; Reinert, F.; Hufner, S.; Grigoryan, V. G.; Springborg, M.; Cercellier, H.; Fagot-Revurat, Y.; Kierren, B.; Malterre, D. *Phys. Rev. B: Condens. Matter Mater. Phys.* **2005**, *72*, 045419.
- (8) Varykhalov, A.; Marchenko, D.; Scholz, M. R.; Rienks, E. D. L.; Kim, T. K.; Bihlmayer, G.; Sánchez-Barriga, J.; Rader, O. *Phys. Rev. Lett.* **2012**, *108*, 066804.
- (9) Koroteev, Y. M.; Bihlmayer, G.; Gayone, J. E.; Chulkov, E. V.; Blugel, S.; Echenique, P. M.; Hofmann, Ph. *Phys. Rev. Lett.* **2004**, *93*, 046403.
- (10) Sugawara, K.; Sato, T.; Souma, S.; Takahashi, T.; Arai, M.; Sasaki, T. *Phys. Rev. Lett.* **2006**, *96*, 046411.
- (11) Dil, J. H.; Meier, F.; Lobo-Checa, J.; Patthey, L.; Bihlmayer, G.; Osterwalder, J. *Phys. Rev. Lett.* **2008**, *101*, 266802.
- (12) Ast, C. R.; Henk, J.; Ernst, A.; Moreschini, L.; Falub, M. C.; Pacilé, D.; Bruno, P.; Kern, K.; Grioni, M. *Phys. Rev. Lett.* **2007**, *98*, 186807.
- (13) Gierz, I.; Suzuki, T.; Frantzeskakis, E.; Pons, S.; Ostanin, S.; Ernst, A.; Henk, J.; Grioni, M.; Kern, K.; Ast, C. R. *Phys. Rev. Lett.* **2009**, *103*, 046803.
- (14) Dedkov, Y. S.; Fonin, M.; Rudiger, U.; Laubschat, C. *Phys. Rev. Lett.* **2008**, *100*, 107602.
- (15) Wang, E.; Tang, P.; Wan, G.; Fedorov, A. V.; Miotkowski, L.; Chen, Y. P.; Duan, W.; Zhou, S. *Nano Lett.* **2015**, *15*, 2031.
- (16) King, P. D. C.; Hatch, R. C.; Bianchi, M.; Ovsyannikov, R.; Lupulescu, C.; Landolt, G.; Slomski, B.; Dil, J. H.; Guan, D.; Mi, J. L.; Rienks, E. D. L.; Fink, J.; Lindblad, A.; Svensson, S.; Bao, S.; Balakrishnan, G.; Iversen, B. B.; Osterwalder, J.; Eberhardt, W.; Baumberger, F.; Hofmann, Ph. *Phys. Rev. Lett.* **2011**, *107*, 096802.
- (17) Zhu, Z.-H.; Levy, G.; Ludbrook, B.; Veenstra, C. N.; Rosen, J. A.; Comin, R.; Wong, D.; Dosanjh, P.; Ubaldini, A.; Syers, P.; Butch, N. P.; Paglione, J.; Elfmov, I. S.; Damascelli, A. *Phys. Rev. Lett.* **2011**, *107*, 186405.
- (18) Eremeev, S. V.; Nechaev, I. A.; Koroteev, Y. M.; Echenique, P. M.; Chulkov, E. V. *Phys. Rev. Lett.* **2012**, *108*, 246802.
- (19) Sakano, M.; Bahramy, M. S.; Katayama, A.; Shimojima, T.; Murakawa, H.; Kaneko, Y.; Malaeb, W.; Shin, S.; Ono, K.; Kumigashira, H.; Arita, R.; Nagaosa, N.; Hwang, H. Y.; Tokura, Y.; Ishizaka, K. *Phys. Rev. Lett.* **2013**, *110*, 107204.
- (20) Kresse, G.; Joubert, D. *Phys. Rev. B: Condens. Matter Mater. Phys.* **1999**, *59*, 1758.
- (21) Kresse, G.; Furthmüller, J. *Comput. Mater. Sci.* **1996**, *6*, 15.
- (22) Perdew, J. P.; Burke, K.; Ernzerhof, M. *Phys. Rev. Lett.* **1996**, *77*, 3865.
- (23) Grimme, S. *J. Comput. Chem.* **2006**, *27*, 1787.
- (24) Heyd, J.; Scuseria, G. E.; Ernzerhof, M. *J. Chem. Phys.* **2003**, *118*, 8207.
- (25) Gomes da Costa, P.; Dandrea, R. G.; Wallis, R. F.; Balkanski, M. *Phys. Rev. B: Condens. Matter Mater. Phys.* **1993**, *48*, 14135.
- (26) Abidri, B.; Ghaffour, M.; Abdellaoui, A.; Bouslama, M.; Hiadsi, S.; Monteil, Y. *Appl. Surf. Sci.* **2010**, *256*, 3007.
- (27) Sanchez-Royo, J. F.; Pellicer-Porres, J.; Segura, A.; Gilliland, S. J.; Safonova, O.; Chevy, A. *Surf. Sci.* **2007**, *601*, 3778.
- (28) Zaoui, X.; Mamy, R.; Chevy, A. *Surf. Sci.* **1988**, *204*, 174.
- (29) Liu, Z.; Liu, C.-X.; Wu, Y.-S.; Duan, W.-H.; Liu, F.; Wu, J. *Phys. Rev. Lett.* **2011**, *107*, 136805.
- (30) Zhou, M.; Liu, Z.; Wang, Z.; Bai, Z.; Feng, Y.; Lagally, M. G.; Liu, F. *Phys. Rev. Lett.* **2013**, *111*, 246801.
- (31) Camara, M. O. D.; Mauger, A.; Devos, I. *Phys. Rev. B: Condens. Matter Mater. Phys.* **2002**, *65*, 125206.
- (32) Nagano, M.; Kodama, A.; Shishidou, T.; Oguchi, T. *J. Phys.: Condens. Matter* **2009**, *21*, 064239.
- (33) Min, H.; Hill, J. E.; Sinitsyn, N. A.; Sahu, B. R.; Kleinman, L.; MacDonald, A. H. *Phys. Rev. B: Condens. Matter Mater. Phys.* **2006**, *74*, 165310.
- (34) Korschuh, S.; Gmitra, M.; Fabian, J. *Phys. Rev. B: Condens. Matter Mater. Phys.* **2010**, *82*, 245412.
- (35) Petersen, L.; Hedegard, P. *Surf. Sci.* **2000**, *459*, 49.
- (36) Ast, C. R.; Gierz, I. *Phys. Rev. B: Condens. Matter Mater. Phys.* **2012**, *86*, 085105.
- (37) Krupin, O. *Dichroism and Rashba effect at magnetic crystal surfaces of rare-earth metals*. Ph.D. Dissertation, Freie Universität, Berlin, 2004.
- (38) Žutić, L.; Fabian, J.; Das Sarma, S. *Rev. Mod. Phys.* **2004**, *76*, 323.
- (39) Mireles, F.; Kirczenow, G. *Phys. Rev. B: Condens. Matter Mater. Phys.* **2001**, *64*, 024426.
- (40) Liu, M.-H.; Chen, S.-H.; Chang, C.-R. *Phys. Rev. B: Condens. Matter Mater. Phys.* **2008**, *78*, 195413.
- (41) Souza, I.; Marzari, N.; Vanderbilt, D. *Phys. Rev. B: Condens. Matter Mater. Phys.* **2001**, *65*, 035109.
- (42) Wang, Z.; Liu, F. *Appl. Phys. Lett.* **2011**, *99*, 042110.
- (43) *Photoelectrochemistry and Photovoltaics of Layered Semiconductors*; Aruchamy, A., Ed.; Kluwer Academic: Netherlands, 1992.
- (44) Zhou, M.; Liu, Z.; Ming, M.; Wang, Z.; Liu, F. *Phys. Rev. Lett.* **2014**, *113*, 236802.
- (45) Zhou, M.; Ming, W.; Liu, Z.; Wang, Z.; Li, P.; Li, F. *PNAS* **2014**, *111*, 14378.